17th World Conference on Earthquake Engineering, 17WCEE
Sendai, Japan - September 13th to 18th 2020

SIMULATION ON NEAR-FIELD PULSE-LIKE GROUND MOTION FOR THE SHUANTUNG FAULT IN TAIWAN REGION

X. L. Chen[(1)], Q. Luo[(2)], M. Gao[(3)], T. Li[(4)]

[(1)] *Professor, Institute of Geophysics, China Earthquake Administration, Beijing 100081, China, e-mail: xueliang_chen@aliyun.com*
[(2)] *Doctor, Institute of Geophysics, China Earthquake Administration, Beijing 100081, China, e-mail:luoquanbo3@163.com*
[(3)] *Professor, Institute of Geophysics, China Earthquake Administration, Beijing 100081, China, e-mail:gaomt1957@163.com*
[(4)] *Doctor, Institute of Geophysics, China Earthquake Administration, Beijing 100081, China, e-mail:2fen222@163.com*

Abstract

Based on the geological and geomorphological characteristics of western Taiwan and the source parameters of the 1999 MW7.6 Chi-Chi earthquake, we have established a 3D velocity structure model and two types of source models. Based on the accumulation of dislocation in the crust and the propagation characteristics of stress and strain after the rock fracture, 3D finite difference method was used to simulate the near-field pulse-like ground motion that can occur in the Shuantung fault activity. The results show that the peak velocity of the horizontal component perpendicular to the fault strike of the strike-slip fault and the vertical component of the reverse fault are large. The double-sided velocity pulses generated by the directivity effect are mainly concentrated in the direction perpendicular to the fault sliding component, while the single-sided velocity pulses generated by the fling-step effect are mainly concentrated in the direction parallel to the fault sliding component. Because of the mutual control of the directivity effect and the hanging wall effect, the near-field pulse-like ground motions exhibit an asymmetrical zonal distribution, and the velocity pulses are mostly distributed within 15 km from the strike-slip fault trace and 10 km from the reverse fault trace. The velocity response spectrum gradually increases along the rupture direction within the coverage of the fault plane, and the velocity pulse may cause severe shear damage to large buildings. Influenced by the characteristics of the asperities, the seismic wave field shows that Nantou, Taichung, and Miaoli are in risk region of strong ground motion. The above study can provides some reference significant for analyzing the mechanism of fault rupture, earthquake prevention and disaster reduction, and earthquake risk analysis.

Keywords: Shuantung fault, pulse-like ground motion, numerical simulation, directivity & fling-step & hanging wall effect, seismic hazard.

1. Introduction

When the causative fault breaks with a velocity close to the shear wave, the huge energy accumulated in the interior of the plate over a long period of time is released instantaneously. Therefore, the station in the near-field region may record a simple waveform, high amplitude, long-period velocity. In recent years, several pulse-like earthquakes occurred in the global, such as the 1994 Northridge M_W6.7 earthquake, the 1995 Kobe M_W6.9 earthquake, and the 2008 Wenchuan M_W7.9 earthquake, all causing severe casualties and economic losses. These loss have caused great concern in the field of seismology and engineering. With the rapid economy development, buildings with large natural vibration period gradually increasing. The study of near-field long-period velocity pulses is of great significance for seismic design and seismic hazard analysis of engineering.

Limited by factors such as the uncertainty of ground motion and the low density of observation instruments, the strong ground database of the Pacific Earthquake Engineering Research Center collected less than 200 pulse records from previous actual earthquake events, making it difficult to obtain the pulse characteristics statistically. With regards to this, researchers have proposed a variety of equivalent velocity pulse models that can better simulate one-side and two-side velocity history curves (Dickinson, Gavin, 2011; Li, 2016; Pu et al., 2017), To a large extent, it compensates for the lack of pulse recordings, but the equivalent velocity pulse model represented by a specific function takes less consideration of the source information. In order to analyze the mechanism of the near-field velocity pulse, pulse-like ground motions are analyzed by the researchers in terms of superimposed the energy, dynamic parameters, and phase difference spectra (Kawase, Aki, 1990; Heaton et al, 1995; Oglesby, Archuleta, 1997), dividing the velocity pulse into directional velocity pulse caused by the Doppler effects and the velocity pulse caused by the slip of the fault. However, the study has mainly analyzed the characteristics of the near-field velocity pulse, and the understanding of its focal mechanism is still insufficient. In order to make up for this deficiency, the researchers used numerical methods to simulate the pulse-like ground motion from the perspective of the source, and verified the feasibility of finite-difference method for near-field ground motion simulation (Gao et al., 2002; Pan et al., 2006; Iwaki et al, 2013; Luo et al, 2019). Numerical simulation results can not only study the causes of near-field ground motion, but also help to analyze the actual response of large structures to velocity pulses.

The numerical simulation of the near-field pulse-like ground motion caused by fault activity has practical significance for the seismic design of the area near the fault. There are many active faults and frequent earthquakes in Taiwan island of China. In 1999, the Chelungpu fault activity in Taiwan stimulated the MW7.6 pulse-like earthquake. Cattin et al. (2004) the convergence rate and the displacement deformation of this fault in geological history, and the results show that the stress of the Shuantung fault located in the upper part of the slip layer increases rapidly during the earthquake intermission. At the same time, Chen et al. (2009) conducted a study on the coseismic displacement distribution and seismic moment release of the Chi-Chi earthquake, indicating that there is a certain relationship between the earthquake and the Shuantung fault, and the region is likely to have another earthquake in the future.

The large earthquake induced by the Shuantung fault has a great influence on the near-field region. The numerical simulation of the near-field pulse-like long-period ground motion has certain theoretical and practical significance. Based on the geological characteristics and detection data of the study area to set up the seismic parameters, and the 3D velocity structure model and the kinematic source model are established. The 3D finite difference method is used to simulate the velocity pulse caused by the Shuantung fault rupture. To compensate for the shortcomings of real-velocity pulse recording from the perspective of source kinematics, and to reveal the mechanism of one-side velocity pulse and two-side velocity pulse, it is proposed to analyze the characteristics of near-field pulse-like ground motion from simulation results, provide some help for earthquake prevention and disaster reduction, earthquake damage assessment and seismic hazard analysis.

2. Simulation area and calculation parameters

2.1 Regional overview

Taiwan is located at the border area between the Eurasian plate and the Philippine plate, and it is the intersection of the Ryukyu trench and the Manila trench, where the plate collision and subduction are relatively strong. A series of strike-slip and inverse faults are formed on the west side of the Central Mountain Range (Yu and Gao, 2001; Wang et al., 2005). The landform structure of Taiwan Island is divided into the coastal mountain belt, the central mountain belt, the western mountain belt, and the western coastal plain belt from east to west. The overall terrain is characterized by high at the east and low at the west. The coastal mountains are composed of Tertiary island arc rocks, the central mountains are mainly composed of the Upper Tertiary metamorphic rocks, the western foothills are mainly composed of the Upper Tertiary Miocene and Pliocene strata, western coastal plain is composed of Quaternary strata with a thickness of about 2 km. The strata east of the Central Mountain Range is relatively old, while the strata in the west are relatively young. There are three thrust faults in the study area (23.37°N~24.58°N, 120.36°E~121.24°E), such as the Shuantung fault, the Chelungpu fault, and the Changhua fault. The distribution is shown in Figure 1. Carena et al. (2002) and Cattin et al. (2004) showed that the Shuantung fault extends down to the main horizontal slip layer about 10 km, and the shortening of the horizontal slip layer is mostly absorbed by the three thrust faults. The slip rate (7~19 mm/a) of the Shuantung fault is between the slip rates of the other two faults, and the earthquake in the future will have a greater probability of exciting the pulse-like ground motion.

2.2 Calculation parameters

The 3D finite difference method in this paper is used to simulate strong ground motion, which is mainly based on the principle of the finite-difference technique. This principle divides the source fault into a finite number of discrete grid elements, according to the slip amount of the subfault, the seismic moment, the rupture time, and the source time function: Eq. (1)

$$f(t) = 2f_c\{1 - \tanh^2 4f_c(t - 1/f_c)\} \tag{1}$$

Where $f(t)$ is a seismic time function, which corresponds to the sliding velocity function on the fault plane; f_c is the characteristic frequency, which is the reciprocal of the fault transition time. The stress and strain components of each grid can be obtained by interpolation calculation, and then the surface motion during the earthquake is simulated. In this paper, a relatively large simulation area is selected. 12 rows (A~L) stations are

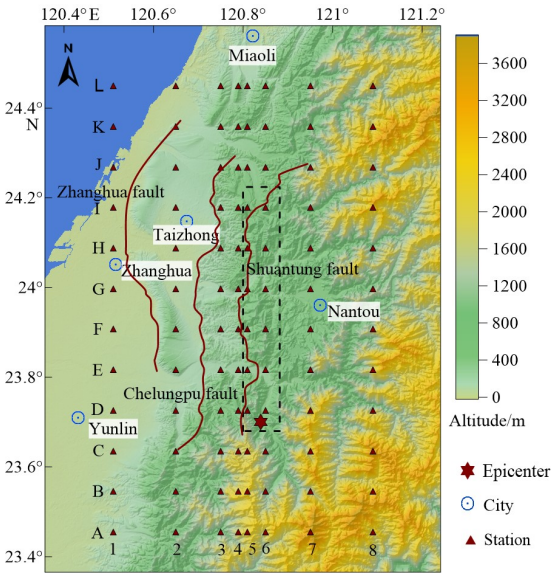

Fig. 1 The distribution of faults (solid lines) in the studied area and the projection of the fault plane at the surface (dashed box) assumed in this paper

arranged perpendicular to the direction of the fault, the spacing between rows is 10 km, 8 stations are arranged along the direction of the fault, and the spacing ranges from 2 to 15 km. In order to better observe the near-field pulse-like ground motion, the stations placed near the fault are denser, and finally 96 stations are deployed on the free surface (Fig. 1). Because the seismic wave velocity of the near-surface sediments in the study area is higher than the wave velocity of the deep medium, the study area is divided into shallow (0-5 km) and deep (5-30 km) in the vertical direction on the premise of ensuring the calculation accuracy. In order to improve the calculation efficiency, the shallow rock near the ground adopts finer grid mesh (grid density is 0.1 km), and the deep rock adopts coarser mesh (grid density is 0.3 km), and the total number of meshes is about 7.2×10^7, and in order to ensure the stability of the calculation, 5 grids for one wavelength under the condition of four-order spatial precision. Since the 3D finite difference method has certain advantages for the simulation of long-period ground motion, in the numerical calculation control parameters, the upper limit frequency is set to 1.4 Hz, the time step is 0.005 s, and the total number of steps is 10,000.

3 Source model and crustal structure model

According to the geometric parameters of the Shuantung fault (Wang et al, 2000) and the empirical statistical relationship by the researchers on the study of the source model (Wells, Coppersmith, 1994; Wang, 2004), this paper sets the possible earthquake magnitude is M_W7. 0, the fault strike is NS, the dip is SE, the dip angle is 45°, the rupture length is 60 km, the width of the fault is 12 km, the source position is 23.68°N, 120.84°E, and the focal depth is about 4 km. The fault propagates in a unilateral circular rupture mode. The fracture propagation velocity is 0.8 times the average shear wave velocity and the rupture time is about 21 s. A single-plane rectangular fault model is established. As shown in Fig. 2, the model is divided into 720 subfaults of 1 km × 1 km, and the entire fault plane is projected on the surface (the dotted line in Fig. 1). Under the same conditions, the left-lateral strike-slip fault with sliding angle of 0° and the reverse fault with sliding angle of 90° were compared to simulate the influence of different focal mechanisms on near-field pulse-like ground motion.

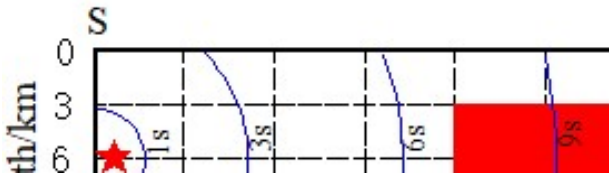

Fig. 2 Sketch of the fault model. The red areas I and II indicate two asperities, the blue arc indicates the rupture model and propagation time

Based on the Eq. (2) proposed by Hanks and Kanamori (1979), determined that the seismic moment of the earthquake in this paper is 3.98×10^{19} Nm.

$$\lg M_0 = 1.5M_W + 16.1 \tag{2}$$

Where M_W is the moment magnitude and M_0 is the seismic moment. The slip amount of the asperities is larger than the average slip of the fault. The number, size and position of the asperities greatly influence the prediction results of strong ground motion. Wang (2004) uses the slip distribution of 29 shallow earthquakes to determine the empirical relationship between the number of asperities and the magnitude, as shown in Eq. (3).

$$N = \mathrm{INT}(2.37M_W - 14.36) \tag{3}$$

Where N is the number of asperities, INT means take an integer. The largest asperity in the multi-asperity model is 0.16 times the area of the entire fault, while the area of other asperities is 0.06 times the area of the fault. Somerville et al. (1999) and Murotani et al. (2008) proposed that the ratio of all the asperities to the entire fault area in the plate boundary earthquakes is close to 0.22, and the average slip of the asperities is 2.2 times the average slip of the entire fault. According to the above relationship, the parameters of the asperities can be set, wherein the number of the asperities is 2, the area of the large asperities I is 120 km^2, and the area of the small asperities II is 42 km^2, and then calculates the seismic moment of the asperities.

$$M_{0a} = \mu D_a S_a \quad (4)$$

In the Eq. (4), M_{0a} is the total seismic moment of the two asperities, D_a is the average slip of the asperities, and S_a is the area of the asperities. The background area is set based on the existing research results of the regional faults (Chi et al, 2001; Luo et al, 2019), due to the fact that the Chi-Chi earthquake excited by the Chelungpu fault and the simulated earthquake excited by the Shuantung are in the same tectonic setting. The rise time of the faults in the background and asperity regions are 3 s and 6 s, respectively.

Ma et al. (1996) obtained the average seismic wave velocity of the crust and upper mantle in Taiwan by the tomography method. Chen et al. (1998) divided the entire island into 26 velocity model blocks based on the variation of S-wave during propagation and local geological structure. Based on the above research results, this paper assumes that the wave velocity, density and Q value are constant of the same horizontal rock formation in the study area, and establishes a 3D crustal velocity structure model. The parameters are listed in Table 1.

Table 1 Structure parameters for the study area

Depth /km	V_P/(km·s^{-1})	V_S/(km·s^{-1})	Density /(10^{3}kg·m^{-3})	Q
2	4.66	2.57	2.25	250
5	5.45	2.67	2.45	250
10	5.76	2.88	2.55	300
15	6.15	3.31	2.60	300
25	6.71	3.72	2.90	500
30	7.11	4.07	3.15	500

4 Simulation results analysis

In this paper, the 3D finite difference simulation of the near-field strong ground motion caused by the Shuantung fault. The pulse-like records are identified from the near-field ground motion according to the velocity pulse criterion proposed by Baker (2007). The velocity time history, the peak ground velocity (PGV), the velocity response spectrum, and the wave field propagation snapshot generated by the strike-slip fault and the reverse fault. It is help to understand the mechanism and distribution characteristics of the velocity pulses.

4.1 velocity time history

The change in near-field ground motion can be represented by its spatial distribution or its attenuation along a certain orientation. In order to compare the velocity time history difference between the strike-slip fault and the reverse fault, qualitative analysis of the three-component velocity time history is carried out in the C5–J5 stations along the fault strike in the region of the hanging wall (1 km) from the fault trace, as shown in Fig. 3. Since the seismic Doppler effect causes the ground motion in the front of rupture are larger than the back of rupture (Benioff, 1955; Hirasawa, Stauder, 1965), it can be seen from Fig. 3 that PGV of the NS component and the EW component in the strike-slip fault is greater than that of the reverse fault, the PGV of the reverse fault in the vertical direction (UD) component is greater than the PGV of the other two components of the fault and the UD component of the strike-slip fault. Velocity pulses are directly related to the directivity effect, fling-step effect, and focal mechanism (Bray, Rodriguez-Marek, 2004; Xie et al., 2012). The energy released by fault rupture accumulates at the front end of the fault in a short of time, and the high-amplitude, long-period, and duration time pulses are reflected on the velocity time history curve. At the front end of the fault, the seismic wave due to fault radiation reaches the surface station for a long time, and the energy is evenly distributed, so the peak value of the near-field ground motion is small and lasts longer (He, 2012). Due to the difference in fault type, different unidirectional pulses and bidirectional pulses are generated in each component. By comparison, it can be found that the unidirectional velocity pulse on the component parallel to strike, and more bidirectional velocity pulses are recorded on the component perpendicular to strike in the strike-slip fault; and more bidirectional velocity pulses on the component parallel to the fault strike, and the other two components record unidirectional velocity

pulses in the reverse fault. The near-field velocity pulse is affected by the fault rupture direction and the sliding direction. Therefore, the bidirectional velocity pulse caused by the directivity effect appears in the direction perpendicular to the fault sliding component, and the unidirectional velocity pulse caused by the fling-step effect appears in the direction parallel to the fault sliding component.

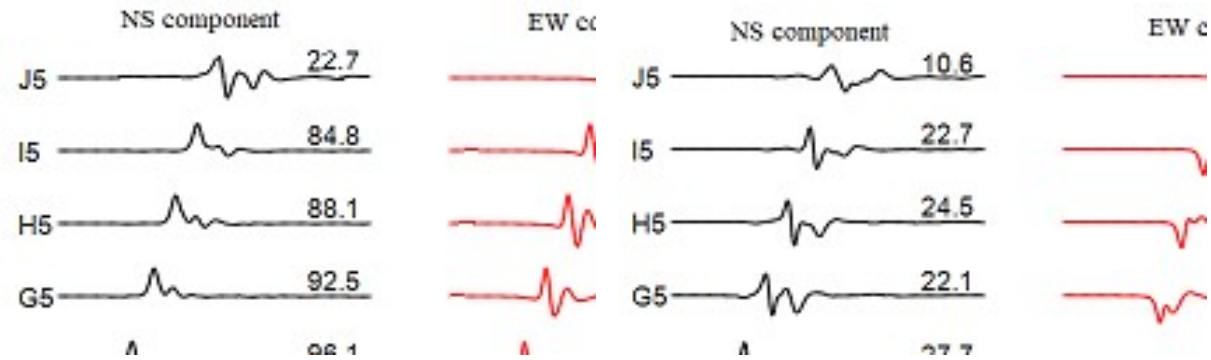

(a) (b)

Fig. 3 Three-component velocity time histories in cm/sec at the stations for strike-slip fault(a)and reverse fault(b)Each subgraph from top to bottom corresponds to the velocity time history of stations such as C5,D5,...,J5

4.2 PGV distribution characteristics

Because it is difficult to obtain quantitative results by the comparison of the velocity time history, it is necessary to compare the peak velocity of the near-field ground motion in both the vertical and parallel directions of the fault, and to analyze the intensity of the velocity pulse by the contours of the peak velocity of the strong ground motion.

Liu et al. (2006) conducted statistics on the seismic damage data of the 1970 Tonghai M_S7.7 earthquake, the 1995 Kobe M_W6.9 earthquake, and the 1999 Kocaeli M_W7.5 earthquake in Turkey. The results show that the attenuation is fast with the increase of the fault distance in the near-field ground motion, and the strong ground motion is mainly distributed in a narrow strip near the fault. Fig. 4 statistics the variation of the three-component peak velocity along the perpendicular to the fault. The logarithmic function is used for regression analysis. From the overall distribution, the peak velocity is different with the distance from the fault. Since the amplitude of the seismic wave is affected by the Mach number of the earthquake, the S-wave transverse amplitude of the vertical fault plane in the near-field region is significantly larger than the radial amplitude of the P-wave in the parallel fault plane (Luo et al., 2018), which makes the component perpendicular to the fault strike has a large peak velocity in the strike-slip fault, reflecting the characteristics of the shear dislocation source radiation effect (Hirasawa and Stauder, 1965; Yuan and Tian, 2012), that is, the amplitude of the near-field ground motion on the component perpendicular to the fault strike is larger, the velocity pulse is also more obvious; the reverse fault is more affected by the dip angle and the fling-step effect of the fault, and the peak velocity is larger in the vertical component. For the strike-slip fault, the peak velocity greater than 30 cm/s is mainly distributed within a range of 15 km from the fault trace; for the reverse fault, the peak velocity distribution range greater than 30 cm/s is relatively small, and the main distribution range is approximately 10 km. Fig. 5 shows the variation of the three-component peak velocity along the fault strike at different stations. It can be seen that the peak velocity in front of the fracture is significantly larger than the peak velocity behind the fracture. The peak velocity gradually increases along the fault as the distance increases. The peak is increased in the range of about 15~60 km from the initial rupture end, and decays after through the end of the fault. In the same range, the peak velocity of different components has different increasing and decreasing along the fault strike. After the fault rupture end, the peak velocity decays faster parallel to the fault strike and vertical components, while the component attenuation perpendicular to the fault strike is slower.

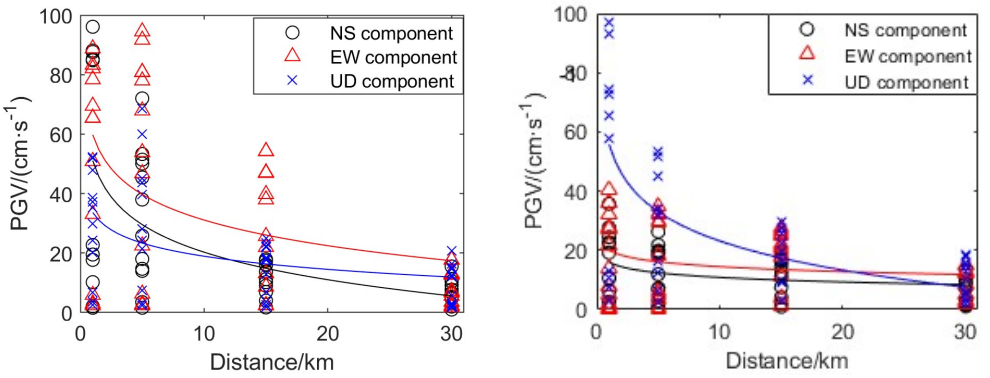

Fig. 4 Variation of three-component peak velocity along the direction perpendicular to the fault strike at the stations of the hanging wall for strike-slip fault (a) and reverse fault (b)

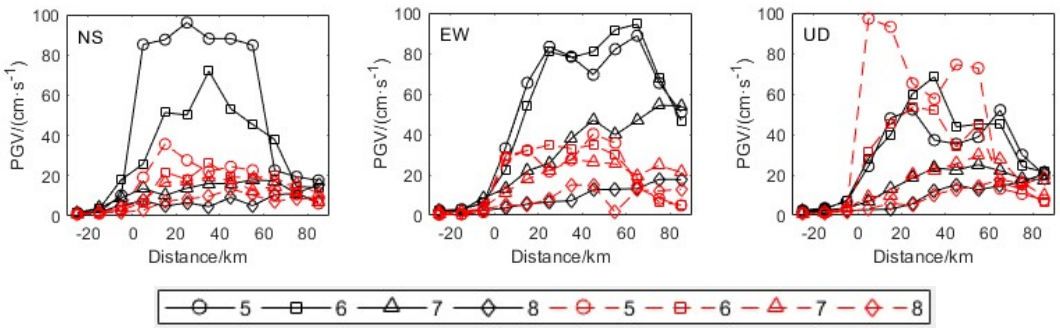

Fig. 5 Variation of three-component peak velocity along the fault strike on the hanging wall for strike-slip fault(solid line)and reverse fault(dashed line)

Using the three pulse-like earthquakes in the simulated earthquake and strong ground motion database, the typical velocity pulse records perpendicular to the strike are selected in the horizontal direction as the basic data of statistical analysis (Table 2), and the distribution characteristics of the pulse peaks with the fault distance are studied. Fig. 6 shows the variation of the 30 simulated records and 52 real records with the fault distance. The velocity pulse obtained by the simulated earthquake is statistically compared with the actual pulses. It can be seen that the pulse peaks decreases with the increase of the fault distance. The simulated pulses are roughly distributed in the real pulses area. Because near-field pulse-like ground motion is affected by many uncertain factors, such as the number of velocity pulse records, the heterogeneity of the propagation medium, and the reflection and refraction of seismic waves caused by complex terrain (Li et al, 2018; Li et al., 2019). Therefore, the macroscopic results of the peak velocity affected by the fault distance still need further study.

Table 2 Parameters of pulse-like earthquakes

Event name	Date	M_W	Number
Imperial Valley earthquake	1979-10-15	6.5	15
Northridge earthquake	1994-01-17	6.7	11
Chi-Chi earthquake	1999-09-21	7.6	26

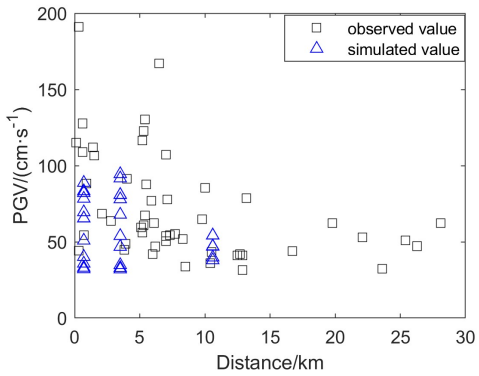

Fig. 6 Distribution of pulse recordings with fault distance for the real earthquakes and simulated earthquake

In order to facilitate the analysis of the spatial variation characteristics of the near-field strong ground motion, the three-component peak velocity contours of the strike-slip fault and the reverse fault are shown in Fig. 7. It can be clearly seen that the directivity effect and the hanging wall effect on the peak size and the distribution range. The directivity effect makes the near-field ground motion spread more widely in the front of rupture, and the attenuation velocity is significantly slower than the back of rupture. At the same time, due to multiple reflections of the seismic wave on the near-field hanging wall, the attenuation of strong ground motion is slower than that of the hanging wall. Therefore, the velocity pulse has a larger peak and a wider distribution range on the hanging wall, reflecting the characteristics of the hanging wall effect (Yu and Gao, 2001; Jiang et al., 2009). Regardless of the strike-slip fault or the reverse fault, it is shown that the ground motion decays faster on the parallel strike and vertical component, while the ground motion attenuation is the slowest on the perpendicular to strike component.

From the numerical simulation results, it is seen that the strong ground motion is concentrated in the vicinity of the fault, which is related to the position of the asperity and the decay rate of the radiated seismic wave of the dislocation source. The near-field region is affected by strong ground motion and surface rupture, which may become a serious earthquake damage area. It can also be seen from the figure that there is strong horizontal ground motion in the near-field region of the strike-slip fault, and the ground motion intensity and influence range generated by the reverse fault in the horizontal direction are relatively small, and the ground motion in the vertical direction is more strong, so it may have a more serious impact on Nantou, Taizhong, and Miaoli. Since the Shuantung fault is located in the western foothill belt, when the long-period velocity pulse generated by the near-field ground motion reaches the natural period of the slope rock mass, which may cause serious geological disasters such as landslides and mudslides.

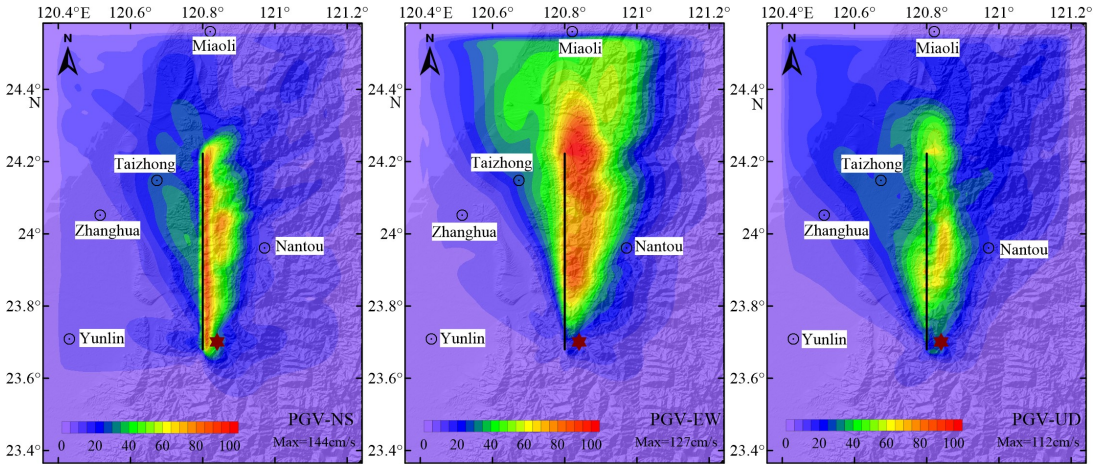

(a)

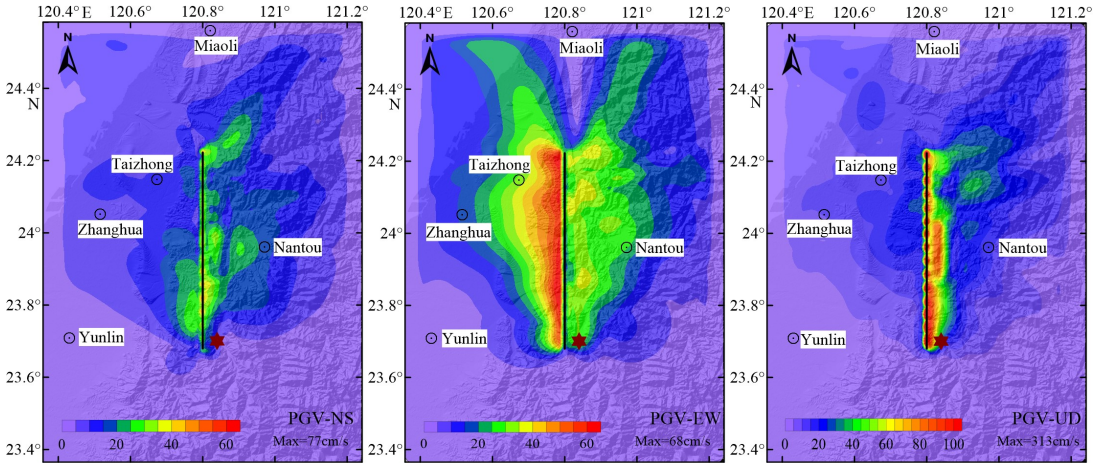

(b)

Fig. 7 Peak velocity contour maps of strike-slip fault(a)and reverse fault(b)

4.3 Velocity response spectrum

The velocity response spectrum of near-field pulse-like ground motion has a long-period characteristic, which has a severe destructive effect on large-scale structures. The velocity can reflect the characteristics of near-field ground motion more than acceleration. The velocity response spectrum also has engineering significance (Xu and Xie, 2005). The characteristic period discussed in this paper is the period value corresponding to the starting down point of the velocity response spectrum curve. Therefore, the three-component velocity response spectrum and the average velocity response spectrum of the stations C5-J5 are calculated by using the damping ratio of 5%, as shown in Fig. 8. It can be seen that the velocity value of each response spectrum increases rapidly with the increase of the period, and then slowly decays after reaches the maximum value, and the response spectrum of

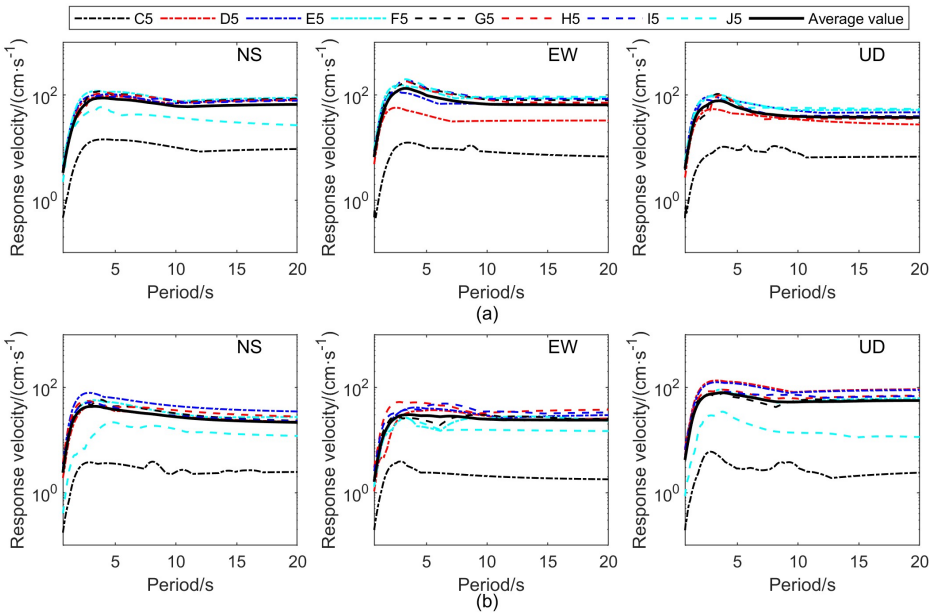

Fig. 8 Three-component velocity response spectrum at the stations for strike-slip fault(a)and reverse fault(b)

each component has an increasing trend along the fault direction. Attenuation occurs again by rupturing the end, which is basically consistent with the results of the peak velocity study. The strike-slip fault has the highest

spectral value on the EW component perpendicular to the fault strike, and the highest spectral value produced by the reverse fault appears on the vertical component. It can be seen from the average velocity response spectrum that the characteristic period of velocity response spectrum in each component is close to the average dislocation rise time over the entire fault plane. The strike-slip fault has the largest characteristic period (about 4.0 s) on the NS component, while there is a maximum characteristic period (about 3.7 s) in the vertical component for the reverse fault. Therefore, large buildings in the near-field region, the velocity pulse caused by the strike-slip fault may produce severe horizontal shear failure due to the resonance effect, and velocity pulses caused by the reverse fault can produce vertical shear damage. By analyzing the change of the velocity spectrum value of the surface station under different periods, we can understand the influence of the near-field velocity pulse on the different natural vibration period structures. Therefore, the study of the pulse-like ground motion is especially important for the seismic and fortification of the engineering structures.

4.4 Seismic wave fields

In order to understand the distribution characteristics of the near-field ground motion in the study area at different

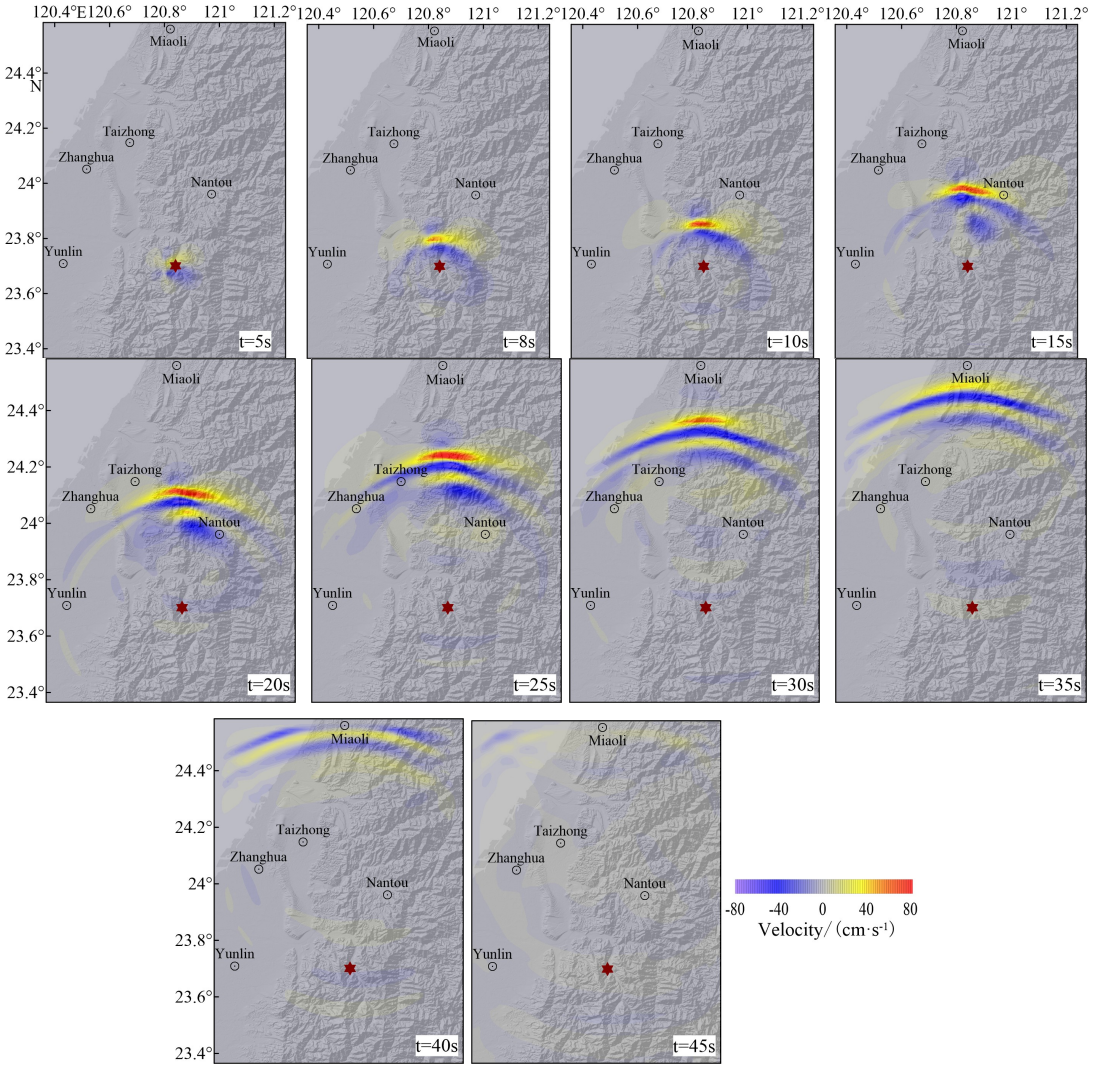

Fig. 9 Snapshots of the wave field at different moments for the ground motion of strike-slip fault

times, we select the wave field propagation snapshot of the EW component of the strike-slip fault for analysis, are shown in Fig. 9. It can be seen that in the initial stage of the earthquake (0~8 s), the strong ground motion is near the epicenter due to the influence of the rock strength, the seismic wave propagation path duration, and the depth of the seismic nucleation zone. Strong ground motion is not obvious, the front end of the fault rupture encounters the large asperity I and the small asperity II in turn after about 8 s, and the intermediate stage (8~35 s)with significant strong ground motion after the earthquake occurs because the fault slip of the asperity area is higher than the background area. Irikura et al. (2017) studied of the 2016 Kumamoto M_W7.0 earthquake and showed that most of the strong ground motions are generated by the asperities, while the contribution of the background area is relatively small; The ground motion decreases as the seismic wave decays outward. From the spatio-temporal characteristics of strong ground motion on the surface, it can be seen that Nantou, Taizhong, and Miaoli may have suffered strong ground motions at the 15th, 20th, and 40th second after the earthquake, respectively, while Yunlin and Zhanghua are located on the footwall. And far from the fault, the impact of strong ground motion is relatively small.

5 Discussion and conclusion

In this paper, the 3D finite-difference method is used to simulate a set earthquake in Taiwan from the perspective of source kinematic, and the prediction results are analyzed. The results show that the simulated velocity pulse is roughly distributed in the real pulse recording region; the velocity time history can better reflect the relationship between the pulse characteristics and the source slip; the peak velocity indicates the distribution of strong ground motion in the near-field region; the velocity response spectra have the difference damage caused by different faults to large structures. The seismic wave fields better indicate the propagation characteristics of seismic waves on the surface and indicates the important areas. However, this method does not simulate the ground motion with a frequency higher than 1 Hz, and there are certain defects in the absorption of seismic waves at the boundary of the simulated region. During the simulation, it is found that reasonable source model and 3D velocity structure model have an important influence on the prediction of near-field pulse-like ground motion. The effective period range, calculation accuracy and efficiency depend on the source time function, the division of subfault, the grid size, and the time step.

By the comparison and analysis of the numerical simulation results for the near-field pulse-like ground motion of the Shuantung fault, the following conclusions are drawn: 1) The large velocity pulse is more likely to appear in the hanging wall and the front of fault. The bidirectional velocity pulse caused by the directivity effect is concentrated in the direction that perpendicular to the slip component of the fault, and the one-side velocity pulse caused by the fling-step effect is mainly concentrated in the direction that parallel to the slip component of the fault. 2) Near-field pulse-like strong ground motion is asymmetrically distributed around the fault. The horizontal component of the strike-slip fault and the vertical component of the reverse fault attenuate faster. The strike-slip fault has a more distributed range of velocity pulses than the reverse fault. It may cause severe horizontal shear damage to large structures, while velocity pulses caused by reverse fault may cause vertical shear damage. 3) The distribution of the asperities and the seismic moment of the subfault affect the spatial and temporal distribution of near-field strong ground motion. Pulse-like ground motions caused by the Shuantung fault may have serious effects on Nantou, Taizhong, and Miaoli.

The simulation records in this paper are basically consistent with the existing results about ground motion, which has certain reference significance for seismic hazard analysis and prediction of pulse-like ground motion. Since this paper does not consider the effects of other rupture modes and site effect, further research is needed in this area to provide a more reliable scientific basis for seismic design of large-scale projects and to minimize the losses caused by earthquakes.

6. Acknowledgements

This research work was supported by Research Institute Foundation: (DQJB19B06); National Science Technology Support Plan Projects: (2012BAK15B01-05), National Natural Science Foundation: (51678537; 51978633; 51278470).

7. The Main References

[1] Baker J W. (2007): Quantitative classification of near-fault ground motions using wavelet analysis. *Bull Seismol Soc Am*, **97**(5) : 1486-1501.

[2] Bray J D, Rodriguez-Marek A. (2004): Characterization of forward-directivity ground motions in the near-fault region. *Soil Dyn Earthq Eng*, **24**(11) : 815-828.

[3] Cattin R, Loevenbruck A, Le Pichon X. (2004) : Why does the co-seismic slip of the 1999 Chi-Chi(Taiwan)earthquake increase progressively northwestward on the plane of rupture ? . *Tectonophysics*, **386**(1/2) : 67-80.

[4] Chen R Y, Kao H, Liang W T, Shin T C, Tsai Y B, Huang B S. (2009): Three-dimensional patterns of seismic deformation in the Taiwan region with special implication from the 1999 Chi-Chi earthquake sequence. *Tectonophysics*, **466**(3/4) : 140-151.

[5] Chi W C, Dreger D, Kaverina A. (2001): Finite-source modeling of the 1999 Taiwan(Chi-Chi)earthquake derived from a dense strong-motion network. *Bull Seismol Soc Am*, **91**(5) : 1144-1157.

[6] Dickinson B W, Gavin H P. (2011): Parametric statistical generalization of uniform-hazard earthquake ground motions. *J Struct Eng*, **137**(3) : 410-422.

[7] Hanks T C, Kanamori H. (1979): A moment magnitude scale. *J Geophys Res*, **84**(B5) : 2348-2350.

[8] Irikura K, Miyakoshi K, Kamae K, Yoshida K, Somei K, Kurahashi S, Miyake H. (2017): Applicability of source scaling relations for crustal earthquakes to estimation of the ground motions of the 2016 Kumamoto earthquake. *Earth Planets Space*, **69**(1) : 10.

[9] Iwaki A, Morikawa N, Maeda T, Aoi S, Fujiwara H. (2013): Finite-difference simulation of long-period ground motion for the Sagami Trough megathrust earthquakes. *J Disaster Res*, **8**(5) : 926-940.

[10] Kawase H, Aki K. (1990): Topography effect at the critical SV-wave incidence : possible explanation of damage pattern by the Whittier Narrows, California, earthquake of 1 October 1987. *Bull Seismol Soc Am*, **80**(1) : 1-22.

[11] Li Z C, Gao M T, Jiang H, Chen X L, Li T F, Zhao X F. (2018): Sensitivity analysis study of the source parameter uncertainty factors for predicting near-field strong ground motion. *Acta Geophys*, **66**(4) : 523-540.

[12] Luo Q B, Chen X L, Gao M T, Li Z C, Zhang Z, Zhou D. (2019): Simulating the near-fault large velocity pulses of the Chi-Chi (Mw7.6) earthquake with kinematic model. *J Seismol*, **23**(1) : 25-38.

[13] Ma K F, Wang J H, Zhao D P. (1996): Three-dimensional seismic velocity structure of the crust and uppermost mantle beneath Taiwan. *J Phys Earth*, **44**(2) : 85-105.

[14] Somerville P, Irikura K, Graves R, Sawada S, Wald D, Abrahamson N, Iwasaki Y, Kagawa T, Smith N, Kowada N. (1999): Characterizing crustal earthquake slip models for the prediction of strong ground motion. *Seismol Res Lett*, **70**(1) : 59-80.

[15] Wells D L, Coppersmith K J. (1994): New empirical relationships among magnitude, rupture length, rupture width, rupture area, and surface displacement. *Bull Seismol Soc Am*, **84**(4) : 974-1002.

